NANO LETTERS

Letter

pubs.acs.org/NanoLett

Metal Nanocrystals Embedded in Single Nanocrystals of MOFs Give Unusual Selectivity as Heterogeneous Catalysts

Kyungsu Na,[†,‡,§,#] Kyung Min Choi,[†,‡,§,#] Omar M. Yaghi,[*,†,‡,§,∥] and Gabor A. Somorjai[*,†,‡,§]

[†]Department of Chemistry, University of California-Berkeley, Berkeley, California 94720, United States

[‡]Lawrence Berkeley National Laboratory, 1 Cyclotron Road, Berkeley, California 94720, United States

[§]Kavli Energy NanoSciences Institute, University of California-Berkeley, Berkeley, California 94720, United States

[∥]Department of Chemistry, King Fahd University of Petroleum and Minerals, Dhahran 34464, Saudi Arabia

Supporting Information

ABSTRACT: The growth of nanocrystalline metal−organic frameworks (nMOFs) around metal nanocrystals (NCs) is useful in controlling the chemistry and metric of metal NCs. In this Letter, we show rare examples of nMOFs grown in monocrystalline form around metal NCs. Specifically, Pt NCs were subjected to reactions yielding Zr(IV) nMOFs [$Zr_6O_4(OH)_4(fumarate)_6$, MOF-801; $Zr_6O_4(OH)_4(BDC)_6$ (BDC = 1,4-benzenedicarboxylate), UiO-66; $Zr_6O_4(OH)_4(BPDC)_6$ (BPDC = 4,4′-biphenyldicarboxylate), UiO-67] as a single crystal within which the Pt NCs are embedded. These constructs $(PtCnMOF)_{nanocrystal}$ are found to be active in gas-phase hydrogenative conversion of methylcyclopentane (MCP) and give unusual product selectivity. The PtCnUiO-66 shows selectivity to C_6-cyclic hydrocarbons such as cyclohexane and benzene that takes place with 100 °C lower temperature than the standard reaction (Pt-**on**-SiO_2). We observe a pore size effect in the nMOF series where the small pore of PtCnMOF-801 does not produce the same products, while the larger pore PtCnUiO-67 catalyst provides the same products but with different selectivity. The $(PtCnMOF)_{nanocrystal}$ spent catalyst is found to maintain the original crystallinity, and be recyclable without any byproduct residues.

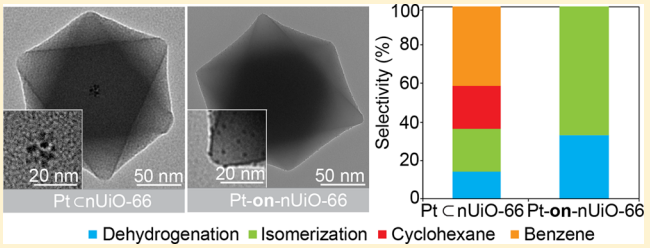

KEYWORDS: *Metal−organic Framework, metal nanocrystal, heterogeneous catalyst, methylcyclopentane, isomerization*

Usually, metal nanocrystals are introduced into the pores of metal−organic frameworks (MOFs) by incorporating metal precursors as guests and reducing them to form the metal nanoparticles.[1−3] These materials have shown interesting catalytic properties but some challenges exist concerning control of metal nanocrystal size, location, and order.[3−8] To express more control over this process a second approach was recently reported where the MOF is grown around preformed metal nanocrystals allowing better control over their metrics.[9−12] However, it remains difficult to control the growth of the MOF in single nanocrystalline form, and thus the MOF is usually grown as polycrystalline around metal nanocrystals.[11−14] This is undesirable for facile diffusion of substrates and products to and from the catalytic sites and often leads to deactivation.[15] In this Letter, we show how Pt nanocrystals can be fully embedded within single crystals of nano MOFs (nMOF-801, nUiO-66, and nUiO-67) with full control over the size and location of the Pt (ca. 2.5 nm) and MOF (ca. 150 nm) nanocrystals. We find that this new $(PtCnMOF)_{nanocrystal}$ construct is capable of carrying out conversion of methylcyclopentane (MCP), a model reaction for selective C−C and C−H bond activation. These conversions occur at 100 °C lower and with higher selectivity to C_6-cyclic products compared to the reference catalyst (Pt supported on mesoporous silica) and also show a MOF pore-dependent activity and selectivity to those products.[16] In addition, the performance, crystallinity, and porosity of this catalyst system are maintained over multiple cycles with no trapped reactants and products found after reactions.

Three members of thermally stable Zr(IV) nMOFs were chosen [$Zr_6O_4(OH)_4(fumarate)_6$, MOF-801; $Zr_6O_4(OH)_4(BDC)_6$ (BDC = 1,4-benzenedicarboxylate), UiO-66; $Zr_6O_4(OH)_4(BPDC)_6$ (BPDC = 4,4′-biphenyldicarboxylate), UiO-67][17,18] and grown as single nanocrystals around Pt nanocrystals (NCs) to make $(PtCnMOF)_{nanocrystal}$ materials. In a typical synthesis, Pt NCs of 2.5 nm size were synthesized using poly(vinylpyrrolidone) (PVP) as a capping agent[19] and were placed in *N*,*N*-dimethylformamide (DMF) solution mixture containing $ZrCl_4$, the respective organic link and acetic acid. This mixture was placed at 120 °C for a day to produce a cloudy solution. This was centrifuged and the nMOF product was collected, washed with DMF and methanol, and dried under vacuum (see Supporting Information for synthesis details). All materials were characterized by powder X-ray

Received: August 5, 2014
Revised: September 3, 2014
Published: September 8, 2014

   dx.doi.org/10.1021/nl503007h | *Nano Lett.* 2014, 14, 5979−5983

diffraction (PXRD), nitrogen gas adsorption, transmission electron microscopy (TEM), and inductively coupled plasma atomic emission spectrometry (ICP-AES). These techniques were used to establish the crystallinity and permanent porosity of nMOFs and the position and amount of Pt NCs. All spent catalysts were analyzed again with PXRD, TEM, and NMR to evaluate their structural and morphological robustness and detect any residues within the catalyst construct.

For each of the nMOFs, TEM images were collected without Pt NCs (nMOF), embedded in the nMOF $(Pt\subset nMOF)_{nanocrystal}$, and, as a control, with Pt NCs on the nMOF (Pt-**on**-nMOF) (see Supporting Information for synthesis details). Figure 1 shows the results for nUiO-66

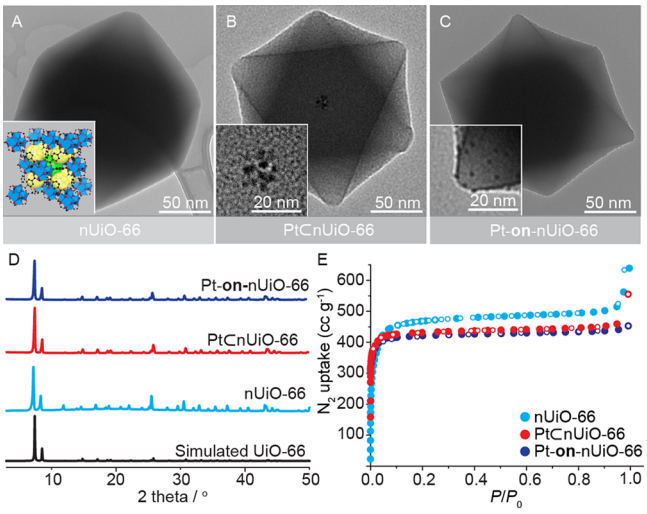

Figure 1. Characterization of nUiO-66, PtCnUiO-66 and Pt-**on**-nUiO-66: (A–C) TEM images, (D) PXRD patterns in comparison with simulated pattern of UiO-66, and (E) N_2 adsorption isotherms at 77 K with adsorption and desorption points represented by closed circles and open circles, respectively (P/P_0, relative pressure).

because its pore size is in the middle of the series (nMOF-801, 5.4 and 7.0 Å; nUiO-66, 6.8 and 7.2 Å; nUiO-67, 9.6 and 12.6 Å). Figure 1A–C clearly shows the single nanocrystallinity of nUiO-66, the Pt NCs embedded in the center of the nUiO-66, and the presence and distribution of Pt NCs on the surface of nUiO-66. No Pt NCs were found to be located on the outside of the nUiO-66 nanocrystals in the $(Pt\subset nMOF)_{nanocrystal}$ as confirmed by Figure 1B. In the case of Pt-**on**-nUiO-66, 2.5 nm Pt NCs were deposited postsynthetically (i.e., after formation of nMOFs) to ensure their location on the outside (Figure 1C and inset).

High crystallinity of nUiO-66, PtCnUiO-66, and Pt-**on**-nUiO-66 is evident from the sharp diffraction lines of their PXRD patterns (Figure 1D), and the coincidence of the diffraction lines between these samples clearly indicates preservation of the bulk UiO-66 structure arrangement for nUiO-66 and upon introduction of Pt NCs in PtCnUiO-66 and Pt-**on**-nUiO-66. The permanent porosity of all these samples is preserved as confirmed by measurement of the N_2 gas-adsorption isotherm, which exhibits a Type I behavior similar to that observed in bulk UiO-66[17] and nUiO-66 (Figure 1E). The corresponding Langmuir surface areas of nUiO-66, PtCnUiO-66 and Pt-**on**-nUiO-66 were calculated to be 2150, 1910, and 1860 $m^2\ g^{-1}$, respectively; values that are also similar to those were found for UiO-66 (1180–2200 $m^2\ g^{-1}$).[17,20,21] ICP-AES revealed that the amounts of Pt for both PtCnUiO-66 and Pt-**on**-nUiO-66 were found to be around 0.4 wt % (see Table S1 in Supporting Information).

Figure 2A shows the schematic reaction pathways of hydrogenative MCP conversion.[16,22] In a typical reaction

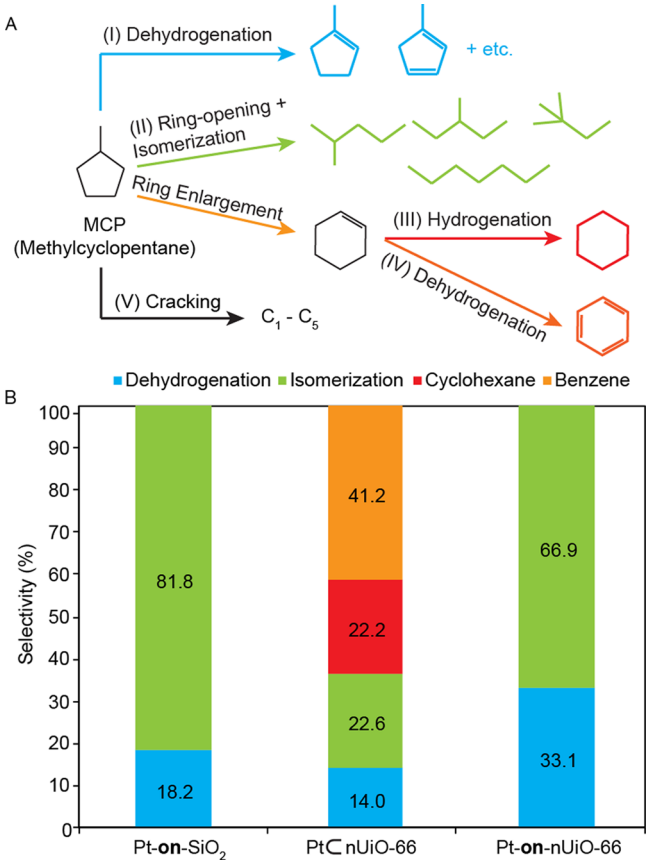

Figure 2. (A) Schematic reaction diagram of hydrogenative conversion of MCP. (B) Product selectivity obtained at 150 °C over three catalysts (Pt-**on**-SiO_2, PtCnUiO-66, and Pt-**on**-nUiO-66).

process, MCP can be converted to various hydrocarbon products via five different reaction pathways. First, MCP can be converted into the dehydrogenated version of MCP through reaction pathway (I). Second, MCP can be ring-opened and isomerized into isomers through reaction pathway (II). The C_5-cyclic ring of MCP can be further enlarged to C_6-cyclic hydrocarbons through ring-enlargement reaction followed with (III) hydrogenation or (IV) dehydrogenation to produce cyclohexane or benzene, respectively. The last reaction pathway is (V) cracking to produce C_1–C_5-based hydrocarbons that are undesired products in this reaction.

Figure 2B shows product selectivity data obtained at 150 °C over nUiO-66 with different locations of Pt NCs in comparison with Pt-**on**-SiO_2 (MCF-17) as the reference catalyst. The study with Pt-**on**-SiO_2 shows the sole catalytic role of Pt NCs because the mesoporous silica support (SiO_2) has no catalytic activity.[22] The Pt-**on**-SiO_2 catalyst can efficiently catalyze the reaction pathways of dehydrogenation and isomerization with selectivities of 18.2 and 81.8%, respectively. No other products were obtained. Similarly, when Pt NCs were supported at the external surface of nUiO-66 crystals, the Pt-**on**-nUiO-66 catalyst can catalyze both dehydrogenation and isomerization with selectivities of 33.1 and 66.9%, respectively. The pure

dx.doi.org/10.1021/nl503007h | Nano Lett. 2014, 14, 5979–5983

nUiO-66 without supporting Pt NCs was also tested for the same reaction, but it showed no catalytic activity. In contrast, when Pt NCs were encapsulated inside the nMOF crystal (Pt⊂nUiO-66), C_6-cyclic hydrocarbon products were predominantly obtained (>60%) with selectivities of 22.2% for cyclohexane (red) and 41.2% for benzene (orange) (Figure 2B). Such a production of C_6-cyclic hydrocarbons at 150 °C is noteworthy because benzene can be produced over Pt-**on**-SiO_2 at higher reaction temperature above 250 °C (see Supporting Information Figure S1 for catalytic results of Pt-**on**-SiO_2).[16] Hence, the facile formation of C_6-cyclic products over Pt⊂nUiO-66 at lower reaction temperature (150 °C) indicates that the embedding Pt NCs in nUiO-66 is contributing to the decrease of activation energy for the formation of C_6-cyclic hydrocarbons.

There are two possibilities for the observed favorable difference in the activity and selectivity of Pt⊂nUiO-66. First, the nMOF structure may assist Pt NCs in making C_6-cyclic hydrocarbons by having the initial products occurring at surface of Pt NCs and further converted over the nUiO-66 porous framework. This is not supported by our findings where pure nUiO-66 showed no activity in the conversion of 2-methylpentane. Instead of 2-methylpentane as a model reactant, we also tested cyclohexene that is known as one of the possible intermediate species during this reaction.[22] However, cyclohexene was not converted over pure nUiO-66 without the presence of Pt NCs. On the basis of these observations, we conclude that the nMOF alone has no catalytic contribution in the absence of Pt NCs. This is because there are no catalytic sites for dissociation of H_2 and activation of hydrocarbon reactant within the nUiO-66 framework. The second possibility is that the micropores in nUiO-66 may accelerate the molecular vibration of reactant or potential transition states, which can lower the activation barrier toward the formation of C_6-cyclic hydrocarbons. Because the kinetic diameters of cyclohexane (6.0 Å) and benzene (5.9 Å) are smaller than the micropores of nUiO-66 (6.8 and 7.2 Å), it would be quite reasonable.[23] More importantly, cyclohexane cannot be formed over Pt-**on**-SiO_2 under the same reaction condition. Hence, the formation of cyclohexane over Pt⊂nUiO-66 might be explained by the increase of local concentration of H_2 inside UiO-66 nanocrystals. Because the diffusion of H_2 into the micropores of nUiO-66 is more facile than the much larger MCP molecule, the H_2 gas should be relatively more localized in the presence of Pt NCs. This in turn would facilitate the production of hydrogenated products. In effect, the nMOF nanocrystals may be acting as a confined nanoreactor wherein the reactants can be localized with H_2 to produce cyclohexane as well as benzene.

In order to investigate the effect of pore size, we also prepared two additional isoreticular (of the same topology) Zr-based nMOFs (nMOF-801 and nUiO-67) with different length of organic links, and thus different pore sizes of the same topology as nUiO-66.[17,18] The micropore sizes progressively increased from nMOF-801 (5.4 and 7.0 Å) to nUiO-66 (6.8 and 7.2 Å) and nUiO-67 (9.6 and 12.6 Å) (Figure 3A).[17,18] Figure 3B shows the selectivity data obtained at 150 °C and how the micropore size plays an important role in product selectivity. Among the three catalysts, the Pt⊂nMOF-801 with the smallest micropore diameter did not give C_6-cyclic hydrocarbons. This catalyst could only make dehydrogenated MCP or ring-opened isomers as observed over the Pt-**on**-SiO_2 catalyst. This is because the pore size of nMOF-801 is smaller

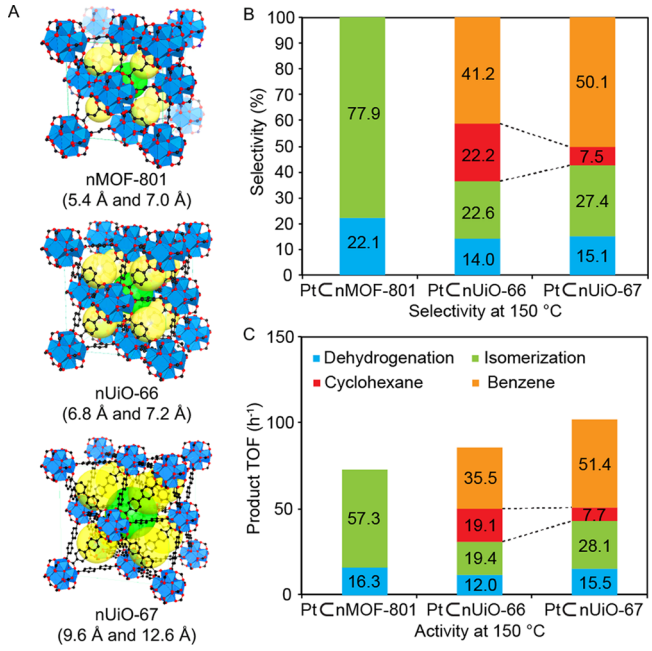

Figure 3. (A) Crystal structure representation of isoreticular Zr-MOFs with different micropore sizes (nMOF-801, nUiO-66, and nUiO-67 from top to bottom). (B) Product selectivity and (C) turnover frequency (TOF, h^{-1}) obtained at 150 °C over Pt⊂nMOF-801, Pt⊂nUiO-66, and Pt⊂nUiO-67.

than kinetic diameters of cyclohexane (6.0 Å) and benzene (5.9 Å). In addition, the adsorption geometries of transition states or intermediate species might be unfavorable toward the formation of C_6-cyclic hydrocarbons within the small micropores of nMOF-801.

However, in the case of Pt⊂nUiO-67 catalyst having the largest micropores, C_6-cyclic hydrocarbons were produced easily as observed over the Pt⊂nUiO-66 catalyst (Figure 3B). The different product selectivity between Pt⊂nUiO-66 and Pt⊂nUiO-67 might originate from the local concentrations of reactant and H_2 inside the nMOF nanocrystals. The catalytic activity data based on the number of Pt sites is shown in Figure 3C. The height of the bar in Figure 3C is the conversion rate of MCP (h^{-1}), which increased progressively with the increase of micropore size. Each bar can be deconvoluted to the product formation rate by multiplying the product selectivity with total TOF of MCP. Among the three catalysts, Pt⊂nMOF-801, Pt⊂nUiO-66, and Pt⊂nUiO-67 produced the largest yield to isomers (57.3 h^{-1}), cyclohexane (19.1 h^{-1}), and benzene (51.4 h^{-1}), respectively.

The harsh reaction conditions and temperature employed to study these reactions prompted us to examine the recyclability of the catalysts and its performance. The recyclability of Pt⊂nUiO-66 is shown in Figure 4A for three consecutive runs under the same reaction conditions expressed above. It is clear from the similarity in TOF numbers that this catalyst construct is stable. The spent catalysts were also evaluated by characterization using PXRD, TEM, and digested NMR. Again, we find that the catalyst is robust and maintains its mononanocrystallinity and morphology after the reaction (Figure 4B,C). The spent catalysts were digested by dissolving it in aqueous HF and analyzed by solution ^{1}H NMR in DMSO-*d6* (Figure 4D). It is clear from the NMR that only the acidified organic link (1,4-benzenedicarboxylic acid) and terminating acetic acid units are shown with no evidence of any other

dx.doi.org/10.1021/nl503007h | *Nano Lett.* 2014, 14, 5979−5983

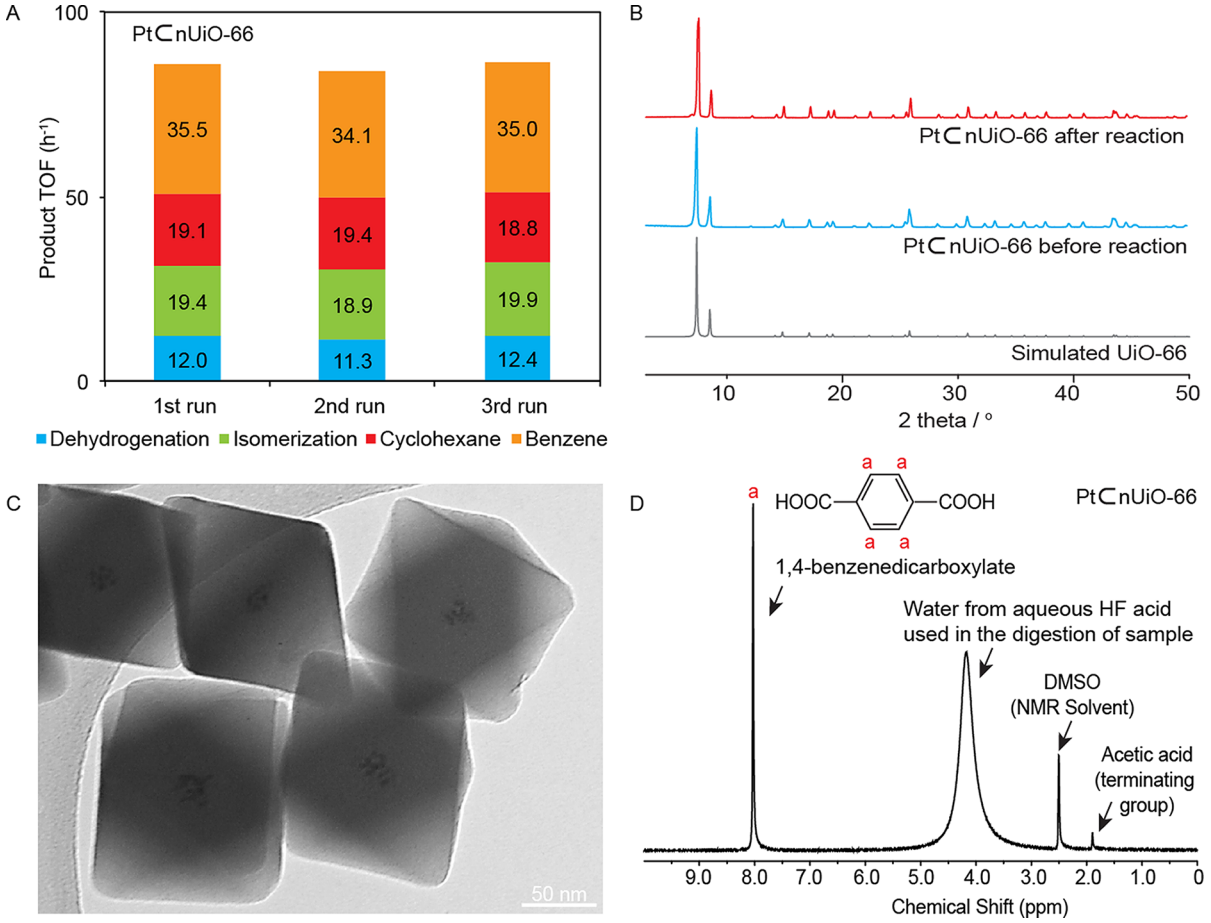

Figure 4. (A) Recyclability of PtCnUiO-66 (no significant changes in product TOF are shown over three times catalytic runs). (B) PXRD patterns of PtCnUiO-66 before (blue) and after reaction (red). (C) TEM image of PtCnUiO-66 after reaction. (D) ^{1}H NMR spectrum of digested PtCnUiO-66 after reaction.

residues that may have deposited inside the catalyst structure after the reaction.

The principal findings of this study clearly indicate that it is possible to make MOF nanocrystals around Pt NCs with the MOF being in monocrystalline form, $(PtCnMOF)_{nanocrystal}$, and that such a construct can be used as a catalyst capable of lowering the temperature of C−C and C−H bond activation reactions by 100 °C and favorably altering product selectivity.

■ ASSOCIATED CONTENT

Supporting Information

Synthesis of catalytic materials, their characterization, and supplementary catalytic reaction results. This material is available free of charge via the Internet at http://pubs.acs.org.

■ AUTHOR INFORMATION

Corresponding Authors

*E-mail: yaghi@berkeley.edu.
*E-mail: somorjai@berkeley.edu.

Author Contributions

#K.N. and K.M.C. contributed equally.

The manuscript was written through contributions of all authors. All authors have given approval to the final version of the manuscript.

Notes

The authors declare no competing financial interest.

■ ACKNOWLEDGMENTS

G.A.S. acknowledges support by The Chevron Energy Technology Company and from the Director, Office of Science, Office of Basic Energy Sciences, Division of Chemical Sciences, Geological, and Biosciences of the U.S. DOE under contract DE-AC02-05CH11231 for catalytic studies. The material synthesis and characterization were supported by BASF SE (Ludwigshafen, Germany) and U.S. Department of Defense, Defense Threat Reduction Agency (HDTRA 1-12-1-0053), respectively. We thank Professor Peidong Yang for use of the TEM instrument.

■ REFERENCES

(1) Hermes, S.; Schröter, M.-K.; Schmid, R.; Khodeir, L.; Muhler, M.; Tissler, A.; Fischer, R. W.; Fischer, R. A. *Angew. Chem., Int. Ed.* **2005**, *44*, 6237.

(2) Meilikhov, M.; Yusenko, K.; Esken, D.; Turner, S.; Tendeloo, G. V.; Fischer, R. A. *Eur. J. Inorg. Chem.* **2010**, *24*, 3701.

(3) Moon, H. R.; Lim, D.; Suh, M. P. *Chem. Soc. Rev.* **2013**, *42*, 1807.

(4) Lu, G.; Li, S.; Guo, Z.; Farha, O. K.; Hauser, B. G.; Qi, X.; Wang, Y.; Wang, X.; Han, S.; Liu, X.; DuChene, J. S.; Zhang, H.; Zhang, Q.; Chen, X.; Ma, J.; Loo, S. C. J.; Wei, W. D.; Yang, Y.; Hupp, J. T.; Huo, F. *Nat. Chem.* **2012**, *4*, 310.

(5) Kuo, C.-H.; Tang, Y.; Chou, L.-Y.; Sneed, B. T.; Brodsky, C. N.; Zhao, Z.; Tsung, C.-K. *J. Am. Chem. Soc.* **2012**, *134*, 14345.

(6) Zhao, M.; Deng, K.; He, L.; Liu, Y.; Li, G.; Zhao, H.; Tang, Z. *J. Am. Chem. Soc.* **2014**, *136*, 1738.

(7) Guo, Z.; Xiao, C.; Maligal-Ganesh, R. V.; Zhou, L.; Goh, T. W.; Li, X.; Tesfagaber, D.; Thiel, A.; Huang, W. *ACS Catal.* **2014**, *4*, 1340.
(8) Li, X.; Guo, Z.; Xiao, C.; Goh, T. W.; Tesfagaber, D.; Huang, W. *ACS Catal.* **2014**, DOI: 10.1021/cs5006635.
(9) Tsuruoka, T.; Kawasaki, H.; Nawafune, H.; Akamatsu, K. *ACS Appl. Mater. Interfaces* **2011**, *3*, 3788.
(10) Falcaro, P.; Hill, A. J.; Nairn, K. M.; Jasieniak, J.; Mardel, J. I.; Bastow, T. J.; Mayo, S. C.; Gimona, M.; Gomez, D.; Whitfield, H. J.; et al. *Nat. Commun.* **2011**, *2*, 237.
(11) Liu, Y.; Tang, Z. *Adv. Mater.* **2013**, *25*, 5819.
(12) Sugikawa, K.; Furukawa, Y.; Sada, K. *Chem. Mater.* **2011**, *23*, 3132.
(13) Silvestre, M. E.; Franzreb, M.; Weidler, P. G.; Shekhah, O.; Wöll, C. *Adv. Funct. Mater.* **2013**, *23*, 1210.
(14) Ke, F.; Qiu, L. G.; Yuan, Y. P.; Jiang, X.; Zhu, J. F. *J. Mater. Chem.* **2012**, *22*, 9497.
(15) Dhakshinamoorthy, A.; Garcia, H. *Chem. Soc. Rev.* **2012**, *41*, 5262.
(16) Alayoglu, S.; Pushkarev, V. V.; Musselwhite, N.; An, K.; Beaumont, S. K.; Somorjai, G. A. *Top. Catal.* **2012**, *55*, 723.
(17) Cavka, J. H.; Jakobsen, S.; Olsbye, U.; Guillou, N.; Lamberti, C.; Bordiga, S.; Lillerud, K. P. *J. Am. Chem. Soc.* **2008**, *130*, 13850.
(18) Wißmann, G.; Schaate, A.; Lilienthal, S.; Bremer, I.; Schneider, A. M.; Behrens, P. *Microporous Mesoporous Mater.* **2012**, *152*, 64.
(19) An, K.; Alayoglu, S.; Musselwhite, N.; Plamthottam, S.; Melaet, G.; Lindeman, A. E.; Somorjai, G. A. *J. Am. Chem. Soc.* **2013**, *135*, 16689.
(20) Choi, K. M.; Jeong, H. M.; Park, J. H.; Zhang, Y.; Kang, J. K.; Yaghi, O. M. *ACS Nano* **2014**, *8*, 7451.
(21) Furukawa, H.; Gandara, F.; Zhang, Y.-B.; Jiang, J.; Queen, W. L.; Hudson, M. R.; Yaghi, O. M. *J. Am. Chem. Soc.* **2014**, *136*, 4369.
(22) Na, K.; Musselwhite, N.; Cai, X.; Alayoglu, S.; Somorjai, G. A. *J. Phys. Chem. A* **2014**, DOI: 10.1021/jp501775q.
(23) Weitkamp, J.; Puppe, L. *Catalysis and Zeolites: Fundamentals and Applications*; Springer: New York, 1999; p 332.